

## Deciphering the 3D Microstructures of a Doubly Charged Homopolymer through a Complementary Correlation of Monomer Crystallography and Polymer Powder X-ray Diffraction

Xi Chen, Glenn A. Spiering, Carla Slebodnick, Timothy E. Long, and Robert B. Moore\*

Cite This: *Macromolecules* 2020, 53, 6529–6537

Read Online

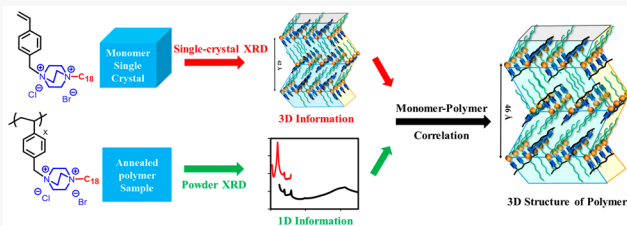
ACCESS |

Metrics & More

Article Recommendations

Supporting Information

**ABSTRACT:** This work unravels the bulk microstructure of a doubly charged homopolymer by correlating crystallographic details from single-crystal X-ray diffraction (SCXRD) of the monomer with the crystalline order of the polymer utilizing powder X-ray diffraction (PXRD). The homopolymer, synthesized through reversible addition–fragmentation chain transfer (RAFT) polymerization, features a styrenic backbone with amphiphilic pendant groups containing a doubly charged 1,4-diazabicyclo[2.2.2]octane (DABCO) salt that is attached to a terminal octadecyl ( $C_{18}$ ) chain. SCXRD of the single crystals grown from the monomers reveals that the amphiphilic monomers prefer to pack into a highly ordered herringbone lamellar structure that facilitates electrostatic interactions between the DABCO salt units and hydrophobic associations of the styrene moieties and pendant  $C_{18}$  chains. Following living radical polymerization from a homogeneous solution, the resulting homopolymer was found to be semicrystalline, despite the expected stereoirregularity (atactic configuration) of the styrenic backbone. Surprisingly, comparisons of the PXRD patterns of the monomer and annealed homopolymer suggest that the homopolymer also crystallizes into a herringbone lamellar structure similar to that of the monomer. Moreover, the V-shaped counterion geometry likely plays an important role in the formation of the herringbone structure for the monomer and the homopolymer to maximize dipole–dipole interactions. Through correlations of the precise crystallographic details of the monomer with the PXRD patterns of the semicrystalline homopolymer, this study highlights a powerful approach in developing a structural model to define the morphology of polymers with complex chemical structures and hierarchical ordering.



### INTRODUCTION

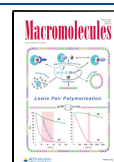
Quaternary ammonium compounds (QACs) are classified as a family of salts that contain at least one ion pair of positive ammonium cations that are electrostatically bonded to free counteranions. The synthesis is achieved through bimolecular nucleophilic substitution reactions of an amine with an alkyl (or benzyl) halide. Polymerization of quaternary ammonium monomers affords ion-containing polymers with positively charged polymer backbones. Typical QAC-based polymers involve imidazolium-, trialkylammonium-, or pyridinium-based cations. These polymers have garnered tremendous attention due to their excellent ionic conductivity compared to other ionic or nonionic counterparts and find potential applications in energy storage such as batteries, supercapacitors, fuel cells, and actuators.<sup>1–4</sup> Imidazolium-based polymers are the most extensively studied category among QAC-polymers, for which the polymer's ionic conductivity has been systematically evaluated as a function of alkyl linkage lengths, counterion types, and backbone structures.<sup>1,2,5–8</sup> The synthesis and physical properties of trialkylammonium-based polymers, including poly(vinylbenzylammonium) and poly(2-(dimethylamino)ethyl methacrylate), have been reported by our group.<sup>9,10</sup> In addition to excellent conductivity, QAC-

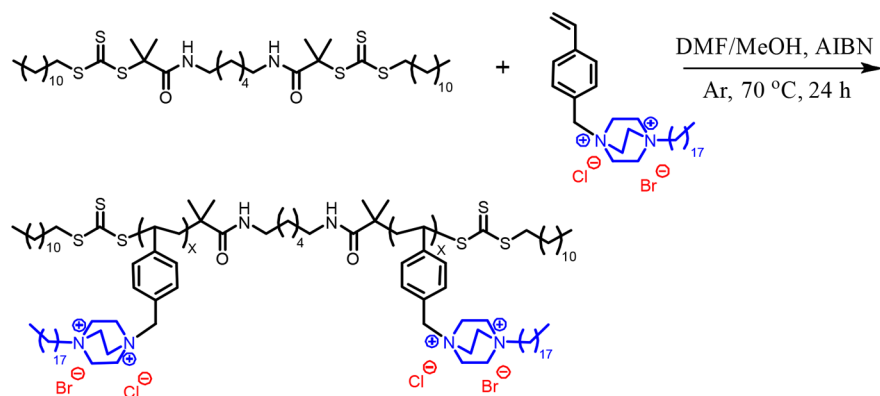
based polymers are also of interest because of their antibacterial efficacy to serve as potential new coatings or membrane materials for biomedical devices, filters, and food processing industries.<sup>11–15</sup> Kawabata and co-workers<sup>14,15</sup> verified efficient elimination of bacteria, yeasts, and fungi using poly(*N*-benzyl-4-vinylpyridinium chloride)-based water filtration membranes. Lu et al. reported the efficacy of poly((dimethylamino)ethyl methacrylate)s against *E. coli* and *S. aureus*.<sup>12</sup> The extensive commercial impacts of charged polymers triggered the development of advanced synthetic avenues to afford novel QAC-based polymers with different compositions, topologies, and architectures,<sup>5,16–23</sup> especially polymers that contain ionic moieties carrying multiple charges in each monomer unit instead of only one cation and anion pair.

Received: June 1, 2020

Revised: July 7, 2020

Published: July 29, 2020



Scheme 1. Synthesis of VBDC<sub>18</sub>BrCl Homopolymer via RAFT Polymerization

The bicyclic organic diamine 1,4-diazabicyclo[2.2.2]octane (DABCO) is receiving increasing attention due to its synthetic versatility. A two-step nucleophilic substitution reaction readily quaternizes the DABCO into doubly charged QACs. High charge density in the DABCO–QACs moiety increases its affinity to negatively charged bacteria cell surfaces compared to the singly charged QACs.<sup>24</sup> Therefore, incorporation of DABCO–QAC functionalities into polymers provides avenues to novel polymers with enhanced antimicrobial performance.<sup>24–27</sup> Yuan et al. synthesized a series of ionenes through randomly linking the DABCO units and the imidazole groups with benzylic or allylic dihalides.<sup>26</sup> *In vitro* assays verified excellent biocompatibility of the polymer and demonstrated the efficacy of the polymer in eliminating a broad range of microbes. Dizman and co-workers<sup>24</sup> developed DABCO-based polymethacrylate homopolymers containing DABCO–QAC pendant units that are attached to alkyl linkers. The homopolymer exhibited resistance against *S. aureus* and *E. coli*, and the antimicrobial activity can be tuned through varying the alkyl linkage lengths. However, most of these works focused on cell culture studies and the solution properties of the DABCO–QAC containing polymers. Reports of the influence of enhanced ionic interactions to the solid-state properties of the polymers are rare. We hypothesize that incorporating strong ionic interactions into the polymers will result in interesting thermal properties, mechanical performance, and morphological behaviors that are significantly different from the singly charged analogues. Therefore, exploring structure–morphology–property relationships of the DABCO–QAC containing polymers is crucial to facilitate a fundamental understanding of the doubly charged polymers at the molecular level.

Recently, our group designed a styrenic DABCO salt containing monomer series (VBDC<sub>x</sub>BrCl) for novel charged polymer synthesis.<sup>17</sup> Zhang et al. randomly copolymerized the DABCO salt monomer with a relatively soft monomer, *n*-butyl acrylate, to produce poly(VBDC<sub>x</sub>BrCl-*co*-nBA) ionic thermoplastic elastomers and studied the effect of concentration, alkyl chain length, and counterion type on the physical properties of the polymers.<sup>16</sup> In our most recent work, we reported the doubly charged ABA triblock copolymer series poly(VBDC<sub>18</sub>BrCl-*b*-nBA-*b*-VBDC<sub>18</sub>BrCl)s with the amphiphilic DABCO salt pendant units in the external blocks.<sup>23</sup> Self-assembly of the block copolymer and strong ionic interactions contributed to a reinforced physical network and led to significantly improved thermomechanical properties compared to the doubly charged random copolymer and singly charged

ABA block copolymer analogues. Small-angle X-ray scattering (SAXS) revealed that the block copolymers phase-separated into a highly ordered, lamellar structure on a large length scale and an interesting secondary ordering within the poly(VBDC<sub>18</sub>BrCl) phase on a smaller scale. However, this secondary ordering remains elusive due to a complicated molecular chemical structure and physical interactions within the poly(VBDC<sub>18</sub>BrCl) phase. Thus, further investigation is necessary to provide a detailed 3D picture of the microstructure within the poly(VBDC<sub>18</sub>BrCl) phase.

Single-crystal X-ray diffraction (SCXRD) is a powerful tool for determining the three-dimensional structure of crystalline solids. Through the identification of a unit cell and atomic coordinates, a 3D structure is produced to allow for analysis of bond length, angles, and packing arrangements. SCXRD is most commonly used to reveal the structure of small molecules or macromolecules including salts, minerals, proteins, and drugs.<sup>28–31</sup> Because most synthetic polymers are semicrystalline or amorphous, it is extremely difficult to obtain polymer single crystals that are large enough for SCXRD. Instead, powder X-ray diffraction (PXRD) is used in the form of both SAXS to assess long-range order and WAXS (wide-angle X-ray scattering) to assess shorter range dimensions. However, with PXRD, the information from a 3D solid is compressed into a 1D scattering profile, hindering the ability to precisely predict 3D structure. Peak overlap and peak broadening due to small crystal sizes also limit the amount and reliability of the information that can be extracted from the PXRD to elucidate polymer microstructure.<sup>32</sup> Most commonly, one determines the distances of the strongest periodicity in semicrystalline and amorphous solids, but the relative directions of the interaction distances to each other in 3D space are lost.

The above limitations of PXRD make it extremely challenging to obtain comprehensive structural information about semicrystalline polymers that cannot form large single crystals required for SCXRD. Although a few studies have suggested that the characteristic structural ordering of the monomers may be retained in the corresponding polymers through comparing the X-ray scattering patterns of the monomer and the polymer,<sup>33,34</sup> a detailed 3D structural analysis of the semicrystalline polymer from SCXRD/PXRD correlations has remained limited. To advance this powerful approach, this work provides a detailed example of a structural analysis of a semicrystalline polymer poly(VBDC<sub>18</sub>BrCl) through correlating the crystallographic details from SCXRD of the VBDC<sub>18</sub>BrCl monomer to the crystalline order of the polymer revealed by PXRD. In-depth structural analysis

demonstrates the poly(VBDC<sub>18</sub>BrCl) is self-assembled into similar structures as the monomer crystal structure, which enables the derivation of a 3D structure model for poly(VBDC<sub>18</sub>BrCl).

## RESULTS AND DISCUSSION

**Polymer Synthesis and Thermal Analysis.** To facilitate the structural ordering of the polymer, we utilized RAFT polymerization (Scheme 1) to afford a more controlled chain propagation and a lower polydispersity that is not achievable with conventional free-radical polymerization.<sup>35,36</sup> An identical difunctional chain transfer agent, diDDMAT-NH<sub>2</sub>, is selected to keep consistency with our previous doubly charged ABA triblock copolymer analogues.<sup>23</sup> Using a DMF/MeOH cosolvent permits the reaction mixture to stay homogeneous throughout the polymerization process. The monomer conversion reached 78% after 24 h of reaction, which was determined by using <sup>1</sup>H NMR in an CD<sub>3</sub>OD/CDCl<sub>3</sub> mixture (Figure S1). Purification through dialysis in a MeOH/CHCl<sub>3</sub> cosolvent for 3 days and subsequent drying *in vacuo* afforded light yellow homopolymer solids that are extremely brittle presumably due to high ionic incorporation and rigid polymer structure. Similar to many ion-containing polymers,<sup>8,20</sup> strong molecular aggregation and solubility difficulty of the homopolymer in common solvents prevent molecular weight analysis using gel permeation chromatography (GPC); therefore, the molecular weight of the homopolymer is estimated based on monomer conversion, which reveals a number-average molecular weight (*M<sub>n</sub>*) of 60.7 kDa.

DSC thermograms in Figure 1 show that both the monomer and the homopolymer exhibit crystalline order. As expected,

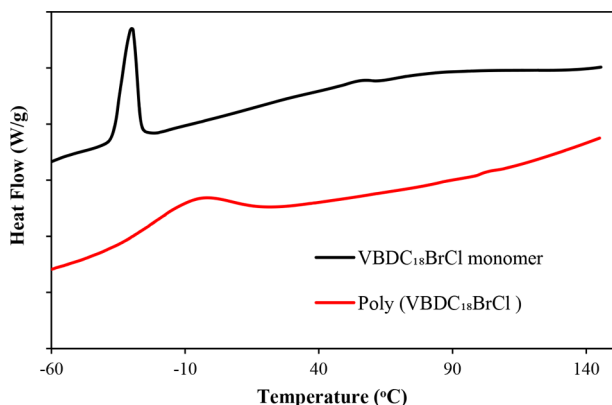


**Figure 1.** DSC thermograms of VBDC<sub>18</sub>BrCl monomer and homopolymer. DSC was performed from  $-80$  to  $140$  °C at  $10$  °C/min under N<sub>2</sub>.

the monomer yields a sharp melting transition attributed to a highly ordered crystalline structure. In contrast, the homopolymer yields a broad endothermic peak located around  $-10$  °C indicative of a less ordered, semicrystalline morphology. The broad endotherm observed in this homopolymer is essentially identical with the endothermic event observed in our previous VBDC<sub>18</sub>BrCl ABA triblock copolymers<sup>23</sup> and has been attributed to the formation C<sub>18</sub> crystalline domains. Despite the expected stereoirregularity of the styrenic backbone, these data suggest that the strongly associating functionalities of the monomer units facilitate the crystalline packing of the pendant alkylated DABCO groups along the polymer chains. While

semicrystalline ordering in other atactic polymers containing small associating groups (e.g., atactic poly(vinyl alcohol)) is known,<sup>37–39</sup> the unexpected ordering of the very large pendant groups in these polymers merits further exploration.

**Monomer Crystal Structure.** Figure 2 illustrates the single-crystal X-ray structure of the VBDC<sub>18</sub>BrCl monomer

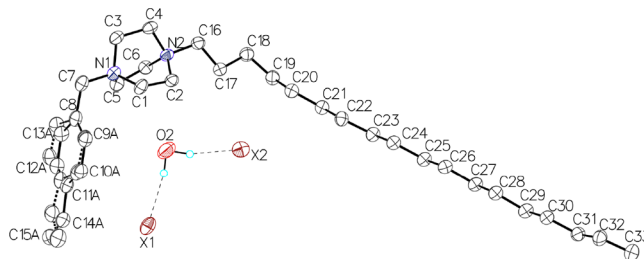


**Figure 2.** Anisotropic displacement ellipsoid drawing (50% probability) and atom labeling diagram for the asymmetric unit of VBDC<sub>18</sub>Br<sub>1.24</sub>Cl<sub>0.76</sub>·H<sub>2</sub>O. Only the major component of the disordered styrene group is labeled. Atoms X1 and X2 represent the compositionally disordered halide Br<sup>−</sup>/Cl<sup>−</sup> halide site. H atoms not involved in hydrogen bonding are omitted for clarity.

determined at 100 K. The monomer crystallizes in the monoclinic space group, *P*2<sub>1</sub>/*c*, with unit cell parameters: *a* = 6.70540(10) Å, *b* = 40.6996(9) Å, *c* = 12.4989(3) Å, β = 93.864(2)°, and *V* = 3403.28(12) Å<sup>3</sup>. The asymmetric unit consists of one monomer dication, two halide anions, and one water molecule of hydration. Both Br<sup>−</sup> and Cl<sup>−</sup> are present at the halide sites (denoted X1 and X2 in the structure) with the relative occupancies refined to give the formula [C<sub>33</sub>H<sub>58</sub>N<sub>2</sub>]<sup>+</sup>Br<sub>1.24</sub>Cl<sub>0.76</sub>·H<sub>2</sub>O. The hydrogen bonds formed between the water and the halides results in a “V-shaped” counterion geometry. In addition, there are some relatively short intermolecular C⋯X and C⋯O distances (Table 1). Except for C17–C18–C19–C20, which adopts a gauche conformation, all torsion angles are anti in the long alkyl pendant unit, forming a planar zigzag chain.

**Table 1.** Closest Nonbonding Interactions for [C<sub>33</sub>H<sub>58</sub>N<sub>2</sub>]<sup>+</sup>Br<sub>1.24</sub>Cl<sub>0.76</sub>·H<sub>2</sub>O [Å and deg]<sup>a</sup>

D–H⋯A	<i>d</i> (D–H)	<i>d</i> (H⋯A)	<i>d</i> (D⋯A)	∠(DHA)
O(2)–H(2C)⋯X(1) <sup>b</sup>	0.99(5)	2.32(5)	3.285(3)	165(4)
O(2)–H(2D)⋯X(2)	1.01(5)	2.23(5)	3.215(3)	166(4)
C(1)–H(1A)⋯O(2)	0.99	2.24	3.039(4)	136.5
C(1)–H(1B)⋯X(2)#1	0.99	2.87	3.687(3)	140.4
C(2)–H(2A)⋯X(1)#1	0.99	2.78	3.638(3)	145.4
C(3)–H(3A)⋯O(2)#1	0.99	2.84	3.673(4)	142.7
C(4)–H(4A)⋯X(1)#2	0.99	2.83	3.685(3)	145.3
C(4)–H(4B)⋯X(1)#1	0.99	2.74	3.658(3)	154.1
C(6)–H(6B)⋯X(1)#2	0.99	2.72	3.621(3)	150.9
C(7)–H(7A)⋯X(2)#1	0.99	2.70	3.625(3)	155.6

<sup>a</sup>Symmetry transformations used to generate equivalent atoms: #1 *x*,  $-y + 1/2$ ,  $z + 1/2$ ; #2 *x*–1,  $-y + 1/2$ ,  $z + 1/2$ . <sup>b</sup>X = halide site with compositional Br and Cl disorder.

Figure 3 highlights the well-ordered packing diagram viewed down the crystallographic *a*-axis. The molecules are arranged into bilayer structures where the favorable interaction between the hydrophilic, doubly charged DABCO units affords distinct regions from the hydrophobic styrenic and alkyl groups. The multiple short-range nonbonding interactions (Table 1) all

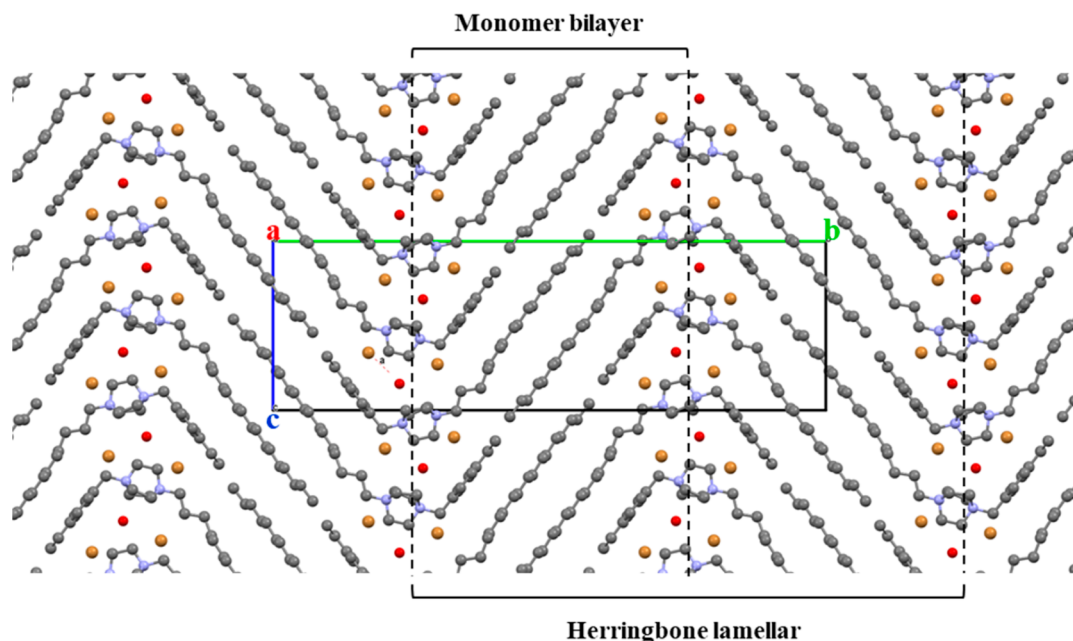


**Figure 3.** View down the crystallographic  $a$ -axis ( $b$ -axis = green,  $c$ -axis = blue). Hydrogen atoms are omitted for clarity. When viewed along the  $c$ -axis, the DABCO orientation alternates left, right, resulting in antiparallel packing of the hydrocarbon chains within the monomer bilayer. The single C17–C18–C19–C20 gauche torsion angle causes a kink in the chain relative to the DABCO group and results in the herringbone packing motif. A network of hydrogen-bonding water and halide atoms separates the DABCO groups of the antiparallel chains. The closest interchain distances are  $\sim 4$  Å.

occur in the hydrophilic regions and help define both the DABCO and hydrocarbon packing arrangements. A  $c$ -glide mirror operation perpendicular to the  $b$ -axis at  $z = 1/2$  relates the adjacent bilayers and oppositely orients the monomer when viewed along the  $c$ -axis. The  $c$ -glides sit at the monomer bilayer markings in Figure 3. When viewed along the  $a$ -axis, the oppositely oriented monomers form interdigitated hydrocarbon regions between the hydrophilic domains. The gauche torsion angle in the octadecyl chain causes a “kink” relative to the DABCO orientation, giving rise to a herringbone lamellar structure. The unit cell parameter  $b$  corresponds to the spacing of each herringbone lamellar unit. Moreover, the DABCO functional groups align parallel to the  $a$ -axis, and the H-bonded water and halides separate the adjacent DABCO units along the  $c$ -axis (Figure 3). Such highly ordered packing is attributed to the amphiphilic nature of the monomer, which facilitate the formation of segregated hydrophobic and hydrophilic domains. In addition, strong noncovalent interactions, including electrostatic dipole–dipole interactions and hydrogen bonding, further promote intra- or interlayer packing, enhancing the structural alignment in three dimensions. Moreover, it is assumed that the V-shaped structure adopted between the water molecule and the halides directs the formation of the herringbone pattern, where the positively charged DABCO unit is preferably positioned with the V-shaped water halides structure to maximize the dipole–dipole interactions. A similar herringbone structure had been revealed for the dialkylimidazolium salt containing a V-shaped pentaiodide ( $I_5^-$ ) counterion.<sup>40</sup> Several other reports also provide evidence for the strong dependency of salt crystal structures on the size or chemical structure of the counterions.<sup>41–43</sup>

**Identification of Characteristic Correlation Spacings within the Monomer Crystal Structure.** Figure 4 compares the PXRD pattern of the bulk monomer powder with a calculated PXRD pattern from the single-crystal X-ray

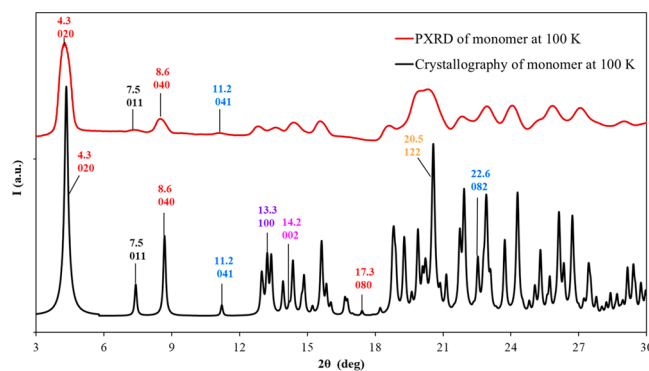


**Figure 4.** Comparison of 100 K bulk monomer PXRD pattern with the powder pattern calculated from the 100 K single-crystal X-ray structure. The indices of some of the Bragg reflections are identified in the single-crystal pattern and correlated to the powder pattern.

structure at 100 K. A select number of indices,  $hkl$ , of the Bragg reflections of the stronger peaks in the calculated single-crystal pattern are also correlated to peaks in the powder pattern. Although the PXRD pattern has broader peaks than the calculated single-crystal pattern due to existence of smaller crystals in the bulk monomer powder and the rapid 5 min scans required to avoid beam damage, a strong agreement exists between peak positions and peak intensities in the two patterns. This confirms that the bulk powder has essentially the same crystalline structure as the single crystal taking into account the peak broadening. The consistency between the patterns means that the high-resolution calculated single-crystal X-ray pattern can be used to identify important interplanar spacings in the monomer and subsequently in the SAXS and WAXS patterns of the polymer (*vide infra*).

Figure 5 depicts the orientation and spacing of the corresponding lattice planes ( $hkl$ ) for three characteristic

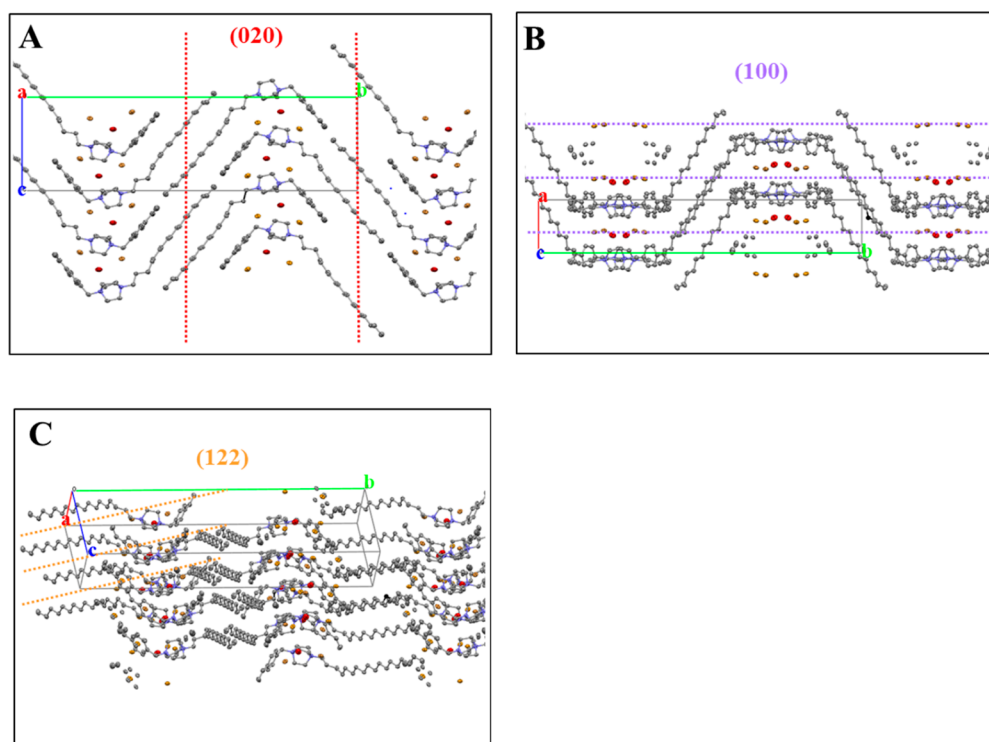


**Figure 5.** Monomer packing diagrams of the single-crystal X-ray structure with significant lattice planes overlaid: (A) (020) planes, (B) (100) planes, and (C) (122) planes. The crystallographic axes are also shown on each image, where *a*-axis = red, *b*-axis = green, and *c*-axis = blue.

diffraction peaks observed in both the SCXRD and PXRD data sets (Figure 4), enabling the identification of important features in the crystal packing diagrams. The (020) planes in Figure 5A have an interplanar distance of 20.35 Å, i.e., half the *b*-axis lattice parameter, which depicts the periodicity of the monomer bilayer in the herringbone structure. Viewing down the *c*-axis (Figure 5B), an interplanar spacing of 6.70 Å between the (100) planes represents the DABCO repeat distance along the *a*-axis. In addition, the packing of C<sub>18</sub> alkyl chains is characterized by the (122) planes, as shown in Figure 5C. The (122) planes aligned with the C<sub>18</sub> alkyl chains have an interplanar spacing of 4.30 Å, corresponding to the distance between alkyl chains in adjacent monomers. Viewing down the *a*-axis (Figure S3), the interplanar spacing for the (082) planes indicates a distance of 3.94 Å for C<sub>18</sub> chains measuring from another direction.

Thermal analysis of the monomer using DSC (Figure 1) reveals an endothermic transition between −40 and −20 °C that is attributed to the melting of the C<sub>18</sub> chain.<sup>23</sup> To probe the temperature effect on the monomer morphology in this phase transition region, we further performed PXRD analysis for the monomer at 223 K (−50 °C) and 300 K (27 °C) (Figure S4). Comparison of the 100, 223, and 300 K PXRD patterns indicates the structure is generally conserved across the temperature range from 100 to 300 K. Noteworthy, all peaks shift slightly to lower scattering angle with increasing temperature, indicating a slight increase of the unit cell parameters attributed to thermal expansion. The unit cell parameters of the single-crystal monomer at 100 and 300 K (Table 2) confirm the thermal expansion of the structure upon heating. The *a*-axis expands the least (0.5%), followed by the *c*-axis (1.2%) and the *b*-axis (2.7%). As the strongest intermolecular interactions occur between the DABCO, H<sub>2</sub>O, and halides, which are parallel to the *a*- and *c*-axis,

**Table 2.** Single-Crystal Unit Cell Parameters of the Monomer at 100 and 300 K

	100 K	300 K
<i>a</i> , Å	6.70540(10)	6.739(6)
<i>b</i> , Å	40.6996(9)	41.801(12)
<i>c</i> , Å	12.4989(3)	12.646(4)
$\alpha$ , deg	90	90
$\beta$ , deg	93.864(2)	93.24(4)
$\gamma$ , deg	90	90
<i>V</i> , Å <sup>3</sup>	3403.28(12)	3557(4)

these dimensions are held together more tightly, and thus the smaller expansion is consistent with the stronger intermolecular interactions of the charged units. Expansion is the greatest parallel to the *b*-axis, i.e., the bilayer lamellar direction associated with the interdigitated antiparallel arrangement of the alkyl chains. In addition, the variable temperature PXRD data in Figure S4 show a subtle reduction in intensity of the (082) peak at 300 K, consistent with a reduction in alkyl chain order at temperatures above the observed melting transition in Figure 1.

The room temperature single-crystal structure of the monomer could not be determined because the sample is susceptible to irreversible structural transition under X-ray exposure over the duration of the experiment (Figure S5). Analysis of styrene packing in the single-crystal structure in Figure S6 also provides convincing evidence for X-ray-induced transformation. The vinyl groups of the monomer single-crystal are aligned appropriately with an interatomic distance of 5.831(10) Å to allow polymerization to occur parallel to the *a*-axis. Solid-state polymerization is a well-known phenomenon that occurs within the monomer single crystal upon photo-irradiation.<sup>44–47</sup>

## Homopolymer and Monomer Structural Correlations.

X-ray scattering profiles in Figure 6 compare the morphology

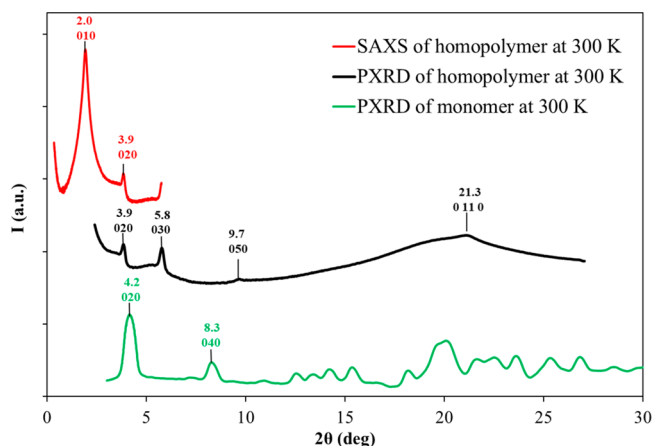


**Figure 6.** Scattering patterns of the homopolymer cast from ethylene glycol/NMP and the monomer at 300 K. Profiles are vertically shifted for clarity.

of the homopolymer and the monomer. For the homopolymer, the SAXS and WAXS patterns reveal sharp scattering maxima at positions consistent with  $1q$ ,  $2q$ ,  $3q$ ,  $5q$ , and  $11q$ , which are indicative of well-ordered lamellar microstructures. The even order reflections are suppressed, exhibiting a lower intensity compared to the odd number reflections, which suggests a nearly symmetric lamellar structure.<sup>48–51</sup> Note that the homopolymer cast from the lower boiling cosolvent (MeOH/CHCl<sub>3</sub>) only reveals broader and lower orders of scattering maxima (up to  $3q$ , Figure S7), which is consistent with faster solvent evaporation leading to the formation of kinetically trapped morphologies.<sup>23,52,53</sup>

A close comparison of the PXRd pattern of the VBDC<sub>18</sub>BrCl monomer and homopolymer at 300 K in Figure 6 shows strong  $0k0$  reflections, implying the homopolymer cast from ethylene glycol/NMP cosolvent is self-assembled into analogous lamellar microstructure as observed in the monomer when viewed parallel to the  $b$ -axis. The scattering maxima for the homopolymer located at  $1q$ ,  $2q$ ,  $3q$ ,  $5q$ , and  $11q$  agree with the periodic arrangement of the  $020$  and  $040$  reflections of the monomer. Note, the  $0k0$ ,  $k = \text{odd}$  reflections for the highly ordered monomer are not observed in the monomer crystal structure because the symmetry of the  $2_1$  screw axis  $\parallel b$  in space group  $P2_1/c$  results in these reflections being systematically absent.

Not surprisingly, the  $0k0$  scattering peaks of the homopolymer shift to lower  $2\theta$  compared to the monomer. This shift indicates an increase in the lamellar dimension from  $\sim 42$  Å for the monomer to  $\sim 46$  Å for the homopolymer. Because the monomer crystal structure represents an energetic minimum in packing arrangement, polymerization would disrupt this packing and increase the lamellar dimension. It is presumed that the slight expansion of the lamellar dimension of the homopolymer compared to the monomer crystal is attributed to styrenic backbone polymerization, where the formation of the stereoirregular single bonds along the backbone disrupts conformational ordering, which is consequently accommodated by an expansion of the lamellar dimension. In addition, the molecular weight distribution of the polymer might cause structural irregularity of the polymer and reduce packing

efficiency. The scattering features between 12 deg and 30 deg for the monomer are replaced with a broad amorphous halo in the homopolymer, suggesting the loss of characteristic monomer scattering dimensions due to polymerization.

## Proposed 3-D Model for the Homopolymer Structure.

Figure 7 depicts a schematic representation of the 3D

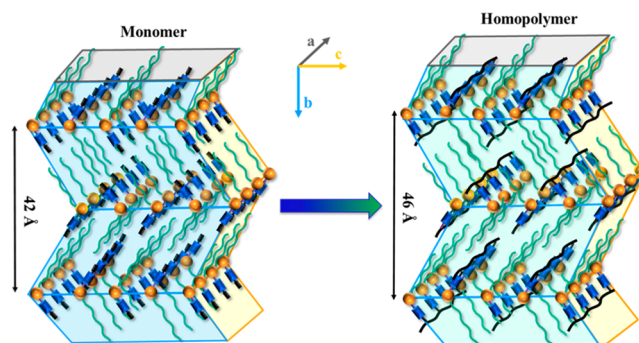


**Figure 7.** Representation of the proposed 3D structure of the VBDC<sub>18</sub>BrCl homopolymer based on the monomer structure. Black = vinyl (monomer) or backbone (polymer), blue = benzene, yellow = DABCO, and green = C<sub>18</sub> chain; the halide ions are not shown for clarity.

structure of the homopolymer. In the proposed structure, the self-assembled homopolymer organizes in the same way as the monomer, with polymer chains packing into well-ordered herringbone lamellar regions parallel to the  $b$ -axis. The pendant alkyl arms of the polymer chain maintain the kinked conformation with respect to the DABCO unit, tilting toward the same orientation and interdigitating with a set of antiparallel alkyl groups from another chain. Moreover, the self-assembled structure alternates on every other interdigitated layer, and one lamellar periodicity is composed of a herringbone unit. This high degree of organization achieved in the homopolymer originates from the strong chemical incompatibility of the pendant moieties, which arranged into separate nanodomains consisting of hydrophilic charged units and hydrophobic styrene and alkyl groups. Moreover, ionic association within the hydrophilic domains and the crystallization within the hydrophobic domains further promote self-assembly and help to define the lamellar structure. Because the ordered morphology stems from the self-assembly of pendant groups and independent of the degree of polymerization ( $N$ ), it provides promising avenues to achieve ordered, sub-10 nm features that are extremely difficult to realize for block copolymers. Similar pendant group organizations had been observed in other semicrystalline polymers such as poly( $n$ -alkylvinylimidazolium)s,<sup>54,55</sup> poly( $n$ -alkyl (meth)acrylate)s,<sup>56,57</sup> and amphiphilic alkyl-containing random copolymers.<sup>58</sup> Noteworthy, our poly(VBDC<sub>18</sub>BrCl) homopolymer demonstrated significantly higher ordering compared to the previous examples, displaying well-defined characteristic scatterings up to  $11q$ . This surprisingly highly ordered structure is presumably attributed to the greater association strength of the doubly charged DABCO-salt units, which serve as strong physical cross-links to improve the packing and reinforce the polymer structure.

## CONCLUSIONS

In summary, we report the synthesis of poly(VBDC<sub>18</sub>BrCl) using RAFT polymerization. The polymer is composed of

styrenic DABCO-based repeating units with the doubly charged QAC moiety and the terminal octadecyl hydrocarbon chain. SCXRD analysis of the monomer at 100 K demonstrates that the monomers organize to maximize interactions between chemically compatible regions to form hydrophilic quaternary ammonium salt regions and hydrophobic styrene and alkyl chain regions. The incompatibility between charged moiety and the nonpolar units drives the self-organization, forming monomer bilayers. Within each hydrophobic region, the octadecyl chains adopt zigzag conformations, which are kinked and interdigitate with a set of antiparallel alkyl chains. The adjacent bilayers are related through a *c*-glide mirror operation, forming an ordered herringbone structure with the lamellar direction parallel to the *b*-axis. The V-shaped geometry formed between water and halides likely templates the formation of the herringbone structure. PXRD of the monomer revealed a consistent crystalline structure compared to SCXRD and enables the measurement of characteristic spacings in the monomer and polymer. Moreover, comparisons of the homopolymer and monomer PXRD pattern suggest that the polymer preserves the lamellar herringbone structure of the monomer with only a slight expansion of the characteristic dimensions. On the basis of the significant agreement between the monomer and polymer X-ray diffraction patterns, a 3D model is proposed for the homopolymer microstructure. This paper illustrates the analytical power of combining high-resolution monomer SCXRD structure with semicrystalline polymer PXRD analysis to deduce the hierarchical structure of a complex self-assembling polymer.

## ■ ASSOCIATED CONTENT

### SI Supporting Information

The Supporting Information is available free of charge at <https://pubs.acs.org/doi/10.1021/acs.macromol.0c01270>.

Experimental section, <sup>1</sup>H NMR spectra of the homopolymer, packing diagram of the monomer single crystal, PXRD of the monomer at varied temperature and time, vinyl groups packing in the monomer single crystal, X-ray scattering of poly(VBDC<sub>18</sub>BrCl) cast from MeOH/CHCl<sub>3</sub> cosolvent (PDF)

Single-crystal structure of VBDC<sub>18</sub>BrCl monomer (CIF)

## ■ AUTHOR INFORMATION

### Corresponding Author

**Robert B. Moore** – Department of Chemistry, Macromolecules Innovation Institute (MII), Virginia Tech, Blacksburg, Virginia 24061, United States; [orcid.org/0000-0001-9057-7695](https://orcid.org/0000-0001-9057-7695);  
Email: [rbmoore3@vt.edu](mailto:rbmoore3@vt.edu)

### Authors

**Xi Chen** – Department of Chemistry, Macromolecules Innovation Institute (MII), Virginia Tech, Blacksburg, Virginia 24061, United States; [orcid.org/0000-0001-6966-6300](https://orcid.org/0000-0001-6966-6300)

**Glenn A. Spiering** – Department of Chemistry, Macromolecules Innovation Institute (MII), Virginia Tech, Blacksburg, Virginia 24061, United States

**Carla Slebodnick** – Department of Chemistry, Macromolecules Innovation Institute (MII), Virginia Tech, Blacksburg, Virginia 24061, United States; [orcid.org/0000-0003-4188-7595](https://orcid.org/0000-0003-4188-7595)

**Timothy E. Long** – Department of Chemistry, Macromolecules Innovation Institute (MII), Virginia Tech, Blacksburg, Virginia 24061, United States; [orcid.org/0000-0001-9515-5491](https://orcid.org/0000-0001-9515-5491)

Complete contact information is available at:  
<https://pubs.acs.org/10.1021/acs.macromol.0c01270>

## Notes

The authors declare no competing financial interest.

## ■ ACKNOWLEDGMENTS

This material is based upon work supported by the National Science Foundation under Grant DMR-1809291. The single-crystal diffractometer was funded by the National Science Foundation under CHE-1726077.

## ■ REFERENCES

- (1) Green, M. D.; Wang, D.; Hemp, S. T.; Choi, J. H.; Winey, K. I.; Heflin, J. R.; Long, T. E. Synthesis of Imidazolium ABA Triblock Copolymers for Electromechanical Transducers. *Polymer* **2012**, *53* (17), 3677–3686.
- (2) Jangu, C.; Wang, J. H. H.; Wang, D.; Sharick, S.; Heflin, J. R.; Winey, K. I.; Colby, R. H.; Long, T. E. Well-Defined Imidazolium ABA Triblock Copolymers as Ionic-Liquid-Containing Electroactive Membranes. *Macromol. Chem. Phys.* **2014**, *215* (13), 1319–1331.
- (3) Kim, T. Y.; Lee, H. W.; Stoller, M.; Dreyer, D. R.; Bielawski, C. W.; Ruoff, R. S.; Suh, K. S. High-Performance Supercapacitors Based on Poly(Ionic Liquid)-Modified Graphene Electrodes. *ACS Nano* **2011**, *5* (1), 436–442.
- (4) Kuray, P.; Noda, T.; Matsumoto, A.; Jacob, C.; Inoue, T.; Hickner, M. A.; Runt, J. Ion Transport in Pendant and Backbone Polymerized Ionic Liquids. *Macromolecules* **2019**, *52* (17), 6438–6448.
- (5) Choi, H.; Ye, Y.; Salas De La Cruz, D.; Liu, W.; Winey, K. I.; Elabd, Y. A.; Runt, J.; Colby, R. H. Dielectric and Viscoelastic Responses of Imidazolium-Based Ionomers with Different Counterions and Side Chain Lengths. *Macromolecules* **2014**, *47*, 777–790.
- (6) Green, M. D.; Salas-De La Cruz, D.; Ye, Y.; Layman, J. M.; Elabd, Y. A.; Winey, K. I.; Long, T. E. Alkyl-Substituted N-Vinylimidazolium Polymerized Ionic Liquids: Thermal Properties and Ionic Conductivities. *Macromol. Chem. Phys.* **2011**, *212* (23), 2522–2528.
- (7) Margareta, E.; Fahs, G. B.; David, L.; Inglefield, J.; Jangu, C.; Wang, D.; Heflin, J. R.; Moore, R. B.; Long, T. E. Imidazolium-Containing ABA Triblock Copolymers as Electroactive Devices. *ACS Appl. Mater. Interfaces* **2016**, *8* (2), 1280–1288.
- (8) Green, M. D.; Long, T. E. Designing Imidazole-Based Ionic Liquids and Ionic Liquid Monomers for Emerging Technologies. *Polym. Rev.* **2009**, *49* (4), 291–314.
- (9) Hemp, S. T.; Zhang, M.; Allen, M. H.; Cheng, S.; Moore, R. B.; Long, T. E. Comparing Ammonium and Phosphonium Polymerized Ionic Liquids: Thermal Analysis, Conductivity, and Morphology. *Macromol. Chem. Phys.* **2013**, *214* (18), 2099–2107.
- (10) Hunley, M. T.; England, J. P.; Long, T. E. Influence of Counteranion on the Thermal and Solution Behavior of Poly (2-(Dimethylamino)Ethyl Methacrylate)-Based Polyelectrolytes. *Macromolecules* **2010**, *43*, 9998–10005.
- (11) Ikeda, T.; Tazuke, S. Biologically Active Polycations: Antimicrobial Activities of Poly [Trialkyl(Vinylbenzyl)Ammonium Chloride]-Type Polycations. *Makromol. Chem., Rapid Commun.* **1983**, *4*, 459–461.
- (12) Lu, G.; Wu, D.; Fu, R. Studies on the Synthesis and Antibacterial Activities of Polymeric Quaternary Ammonium Salts from Dimethylaminoethyl Methacrylate. *React. Funct. Polym.* **2007**, *67*, 355–366.
- (13) Senuma, M.; Tashiro, T.; Iwakura, M.; Kaeriyama, K.; Shimura, Y. Synthesis and Antibacterial Activity of Copolymers Having a Quaternary Ammonium Salt Side Group. *J. Appl. Polym. Sci.* **1989**, *37*, 2837–2843.
- (14) Kawabata, N.; Fujita, I.; Inoue, T. Removal of Virus from Water by Filtration Using Microporous Membranes Made of Made of

Poly(N-Benzyl-4-Vinylpyridinium Chloride). *J. Appl. Polym. Sci.* **1996**, *60*, 911–917.

(15) Kawabata, N.; Nishiguchi, M. Antibacterial Activity of Soluble Pyridinium-Type Polymers. *Appl. Environ. Microbiol.* **1988**, *54* (10), 2532–2535.

(16) Zhang, K.; Fahs, G. B.; Drummey, K. J.; Moore, R. B.; Long, T. E. Doubly-Charged Ionomers with Enhanced Microphase-Separation. *Macromolecules* **2016**, *49* (18), 6965–6972.

(17) Zhang, K.; Drummey, K. J.; Moon, N. G.; Chiang, W. D.; Long, T. E. Styrenic DABCO Salt-Containing Monomers for the Synthesis of Novel Charged Polymers. *Polym. Chem.* **2016**, *7*, 3370–3374.

(18) Zhao, Q.; Shen, C.; Halloran, K. P.; Evans, C. M. Effect of Network Architecture and Linker Polarity on Ion Aggregation and Conductivity in Precise Polymerized Ionic Liquids. *ACS Macro Lett.* **2019**, *8*, 658–663.

(19) Weiss, R. A.; Sen, A.; Pottick, L. A.; Willis, C. L. Block Copolymer Ionomers: 2. Viscoelastic and Mechanical Properties of Sulphonated Poly(Styrene-Ethylene/Butylene-Styrene). *Polymer* **1991**, *32* (15), 2785–2792.

(20) Deng, G.; Cavicchi, K. A. Tuning the Viscoelastic Properties of Poly(n-Butyl Acrylate) Ionomer Networks through the Use of Ion-Pair Comonomers. *Macromolecules* **2017**, *50* (23), 9473–9481.

(21) Storey, R. F.; Chisholm, B. J.; Lee, Y. Synthesis and Mechanical Properties of Poly(Styrene-*b*-Isobutylene-*b*-Styrene) Block Copolymer Ionomers. *Polym. Eng. Sci.* **1997**, *37* (1), 73–80.

(22) Park, M. J.; Balsara, N. P. Phase Behavior of Symmetric Sulfonated Block Copolymers. *Macromolecules* **2008**, *41*, 3678–3687.

(23) Chen, X.; Talley, S. J.; Haag, J. V.; Spiering, G. A.; Liu, B.; Drummey, K. J.; Murayama, M.; Moore, R. B.; Long, T. E. Doubly Charged ABA Triblock Copolymers: Thermomechanically Robust Physical Network and Hierarchical Microstructures. *Macromolecules* **2019**, *52*, 9168–9176.

(24) Dizman, B.; Elasmri, M. O.; Mathias, L. J. Synthesis and Antimicrobial Activities of New Water-Soluble Bis-Quaternary Ammonium Methacrylate Polymers. *J. Appl. Polym. Sci.* **2004**, *94* (2), 635–642.

(25) Pappas, H. C.; Sylejmani, R.; Graus, M. S.; Donabedian, P. L.; Whitten, D. G.; Neumann, K. Antifungal Properties of Cationic Phenylene Ethynyls and Their Impact on  $\beta$ -Glucan Exposure. *Antimicrob. Agents Chemother.* **2016**, *60* (8), 4519–4529.

(26) Yuan, Y.; Liang, S.; Li, J.; Zhang, S.; Zhang, Y. Copolymers with Both Soft and Rigid Cationic Rings as Highly Selective Antimicrobials to Combat Antibiotic Resistant Microbes and Biofilms. *J. Mater. Chem. B* **2019**, *7*, 5620–5625.

(27) Lall, S.; Behaj, V.; Mancheno, D.; Casiano, R.; Thomas, M.; Rikin, A.; Gaillard, J.; Raju, R.; Scumpia, A.; Castro, S.; Engel, R.; Cohen, J. I. Polycations-12. The Synthesis of Liquid Ionic Phosphates (LIPs) from Mono- and Polycationic Ammonium Halides. *Synthesis* **2002**, *11*, 1530–1540.

(28) Volkmer, D.; Mayr, N.; Fricke, M. Crystal Structure Analysis of [Ca(O3SC18H37)2(DMSO)2], a Lamellar Coordination Polymer and Its Relevance for Model Studies in Biomineralization. *Dalton Trans.* **2006**, 4889–4895.

(29) Böcskei, Z.; Groom, C. R.; Flower, D. R.; Wright, C. E.; Phillips, S. E. V.; Cavagioni, A.; Findlay, J. B. C.; North, A. C. T. Pheromone Binding to Two Rodent Urinary Proteins Revealed by X-Ray Crystallography. *Nature* **1992**, *360* (6400), 186–188.

(30) Lopez, C.; Claramunt, R. M.; Sanz, D.; Foces, C. F.; Cano, F. H.; Faure, R.; Cayon, E.; Elguero, J. Structure of Bis-, Tris- and Tetrakispyrazolylborates in the Solid State (Sodium and Potassium Salts of Tetrakispyrazolylborate by X-Ray Crystallography) and in Solution (1H, 11B, 13C and 15N NMR). *Inorg. Chim. Acta* **1990**, *176* (2), 195–204.

(31) Ding, X.; Zeng, H.; Schiering, N.; Ringe, D.; Murphy, J. R. Identification of the Primary Metal Ion-Activation Sites of the Diphtheria Tox Repressor by X-Ray Crystallography and Site-Directed Mutational Analysis. *Nat. Struct. Mol. Biol.* **1996**, *3* (4), 382–387.

(32) Li, J.; Sun, J. Application of X-Ray Diffraction and Electron Crystallography for Solving Complex Structure Problems. *Acc. Chem. Res.* **2017**, *50* (11), 2737–2745.

(33) Bunz, U. H. F.; Enkelmann, V.; Kloppenburg, L.; Jones, D.; Shimizu, K. D.; Claridge, J. B.; Loye, H. Solid-State Structures of Phenyleneethynyls: Comparison of Monomers and Polymers. *Chem. Mater.* **1999**, *11* (3), 1416–1424.

(34) Wu, Q.; Lv, C.; Zhang, Z.; Li, Y.; Nie, J.; Xu, J.; Du, B. Poly(N-Isopropylacrylamide-Co-1-Vinyl-3-Alkylimidazolium Bromide) Microparticles with Internal Nanophase-Separated Structures. *Langmuir* **2018**, *34*, 9203–9214.

(35) Keddie, D. J.; Moad, G.; Rizzardo, E.; Thang, S. H. RAFT Agent Design and Synthesis. *Macromolecules* **2012**, *45* (13), 5321–5342.

(36) Moad, G.; Rizzardo, A. E.; Thang, S. H. Living Radical Polymerization by the RAFT Process. *Aust. J. Chem.* **2005**, *58*, 379–410.

(37) Kenney, J. F.; Willcockson, G. W. Structure-Property Relationships of Poly (Vinyl Alcohol). 111. Relationships between Stereo- Regularity, Crystallinity, and Water Resistance in Poly (Vinyl Alcohol). *J. Polym. Sci., Part A-1: Polym. Chem.* **1966**, *4*, 679–698.

(38) Assender, H. E.; Windle, A. H. Crystallinity in Poly(Vinyl Alcohol). 1. An X-Ray Diffraction Study of Atactic PVOH. *Polymer* **1998**, *39* (18), 4295–4302.

(39) Guerrero, A. H.; Williams, R. T. The Tollens Naphthoresorcinol Reaction for Uronic Acids [7]. *Nature* **1948**, *161* (4102), 930–931.

(40) Wang, X.; Vogel, C. S.; Heinemann, F. W.; Wasserscheid, P.; Meyer, K. Solid-State Structures of Double-Long-Chain Imidazolium Ionic Liquids: Influence of Anion Shape on Cation Geometry and Crystal Packing. *Cryst. Growth Des.* **2011**, *11* (5), 1974–1988.

(41) Wang, X.; Heinemann, F. W.; Yang, M.; Melcher, B. U.; Fekete, M.; Mudring, A. V.; Wasserscheid, P.; Meyer, K. A New Class of Double Alkyl-Substituted, Liquid Crystalline Imidazolium Ionic Liquids - A Unique Combination of Structural Features, Viscosity Effects, and Thermal Properties. *Chem. Commun.* **2009**, No. 47, 7405–7407.

(42) Okuyama, K.; Ishii, T.; Vongbupnimit, K.; Noguchi, K. Structural Studies of Cetyltrimethylammonium Chloride and Its Complex with *p*-Phenylphenol. *Mol. Cryst. Liq. Cryst. Sci. Technol., Sect. A* **1998**, *312*, 101–115.

(43) Sawada, K.; Kitamura, T.; Ohashi, Y.; Iimura, N.; Hirata, H. X-Ray Analysis of Complexes Formed between Surfactants and Aromatic Compounds. I. A Common Structural Pattern of the Complexes. *Bull. Chem. Soc. Jpn.* **1998**, *71*, 2109–2118.

(44) Tashiro, K.; Kusaka, K.; Hosoya, T.; Ohhara, T.; Hanesaka, M.; Yoshizawa, Y.; Yamamoto, H.; Niimura, N.; Tanaka, I.; Kurihara, K.; et al. Structure Analysis and Derivation of Deformed Electron Density Distribution of Polydiacetylene Giant Single Crystal by the Combination of X-Ray and Neutron Diffraction Data. *Macromolecules* **2018**, *51* (11), 3911–3922.

(45) Tashiro, K.; Yamamoto, H.; Sugimoto, K.; Takahama, T.; Tanaka, M.; Hasegawa, M. Experimental Determination of the Geometrical Relation between Monomer and Polymer Species of 2,5-Distyrylpyrazine Single Crystal in the Topotactic Photoinduced Polymerization Reaction. *Macromolecules* **2019**, *52*, 2189–2202.

(46) Matsumoto, A.; Yokoi, K.; Aoki, S.; Tashiro, K.; Kamae, T.; Kobayashi, M. Crystalline-State Polymerization of Diethyl (*Z,Z*)-2,4-Hexadienedioate via a Radical Chain Reaction Mechanism To Yield an Ultrahigh-Molecular-Weight and Stereoregular Polymer. *Macromolecules* **1998**, *31* (7), 2129–2136.

(47) Saragai, S.; Tashiro, K.; Nakamoto, S.; Matsumoto, A.; Tsubouchi, T. Relationship between Packing Structure and Monomer Reactivity in the Photoinduced Solid-State Polymerizations of Muconic Diesters with Different Side Groups. *J. Phys. Chem. B* **2001**, *105*, 4155–4165.

(48) Burger, C.; Micha, M. A.; Oestreich, S.; Förster, S.; Antonietti, M. Characterization of Two New Stable Block Copolymer

Mesophases by Synchrotron Small-Angle Scattering. *Europhys. Lett.* **1998**, *42* (4), 425–429.

(49) Kane, L.; Satkowski, M. M.; Smith, S. D.; Spontak, R. J. Phase Behavior and Morphological Characteristics of Compositionally Symmetric Diblock Copolymer Blends. *Macromolecules* **1996**, *29* (27), 8862–8870.

(50) Bockstaller, B. M.; Kolb, R.; Thomas, E. L. Metalodielectric Photonic Crystals Based on Diblock Copolymers. *Adv. Mater.* **2001**, *13*, 1783–1786.

(51) Lynd, N. A.; Hamilton, B. D.; Hillmyer, M. A. The Role of Polydispersity in the Lamellar Mesophase of Model Diblock Copolymers. *J. Polym. Sci., Part B: Polym. Phys.* **2007**, *45*, 3386–3393.

(52) Chen, X.; Zhang, K.; Talley, S. J.; Orsino, C. M.; Moore, R. B.; Long, T. E. Quadruple Hydrogen Bonding Containing Supramolecular Thermoplastic Elastomers: Mechanical and Morphological Correlations. *J. Polym. Sci., Part A: Polym. Chem.* **2019**, *57* (1), 13–23.

(53) Moore, R. B.; Martin, C. R. Procedure for Preparing Solution-Cast Perfluorosulfonate Ionomer Films and Membranes. *Anal. Chem.* **1986**, *58*, 2569–2570.

(54) Salas-De La Cruz, D.; Green, M. D.; Ye, Y.; Elabd, Y. A.; Long, T. E.; Winey, K. I. Correlating Backbone-to-Backbone Distance to Ionic Conductivity in Amorphous Polymerized Ionic Liquids. *J. Polym. Sci., Part B: Polym. Phys.* **2012**, *50* (5), 338–346.

(55) Yuan, J.; Soll, S.; Drechsler, M.; Muller, A. H. E.; Antonietti, M. Self-Assembly of Poly(Ionic Liquid)s: Polymerization, Mesostructure Formation, and Directional Alignment in One Step. *J. Am. Chem. Soc.* **2011**, *133*, 17556–17559.

(56) Beiner, M.; Huth, H. Nanophase Separation and Hindered Glass Transition in Side-Chain Polymers. *Nat. Mater.* **2003**, *2* (9), 595–599.

(57) Arbe, A.; Genix, A. C.; Colmenero, J.; Richter, D.; Fouquet, P. Anomalous Relaxation of Self-Assembled Alkyl Nanodomains in High-Order Poly(n-Alkyl Methacrylates). *Soft Matter* **2008**, *4* (9), 1792–1795.

(58) Hattori, G.; Takenaka, M.; Sawamoto, M.; Terashima, T. Nanostructured Materials via the Pendant Self-Assembly of Amphiphilic Crystalline Random Copolymers. *J. Am. Chem. Soc.* **2018**, *140*, 8376–8379.